Hindawi
Journal of Nanotechnology
Volume 2022, Article ID 3693938, 9 pages
https://doi.org/10.1155/2022/3693938

Research Article

Bentonite Nanoclay Optoelectrochemical Property Improvement through Bimetallic Silver and Gold Nanoparticles

Sizwe Ngcobo, Bongiwe Silwana, Kanyisa Maqhashu, and Mangaka C. Matoetoe

Department of Chemistry, Cape Peninsula University of Technology, Tennant Street, P.O. Box 652, Cape Town, South Africa

Correspondence should be addressed to Mangaka C. Matoetoe; lellangm@gmail.com

Received 16 May 2022; Revised 20 July 2022; Accepted 8 September 2022; Published 3 October 2022

Academic Editor: Marco Rossi

This study assesses the physical and electrochemical changes of bimetallic Ag-Au nanoparticle-functionalized bentonite nanoclay. Nanoclay was studied to deduce a better sensing material/film. A chemical co-reduction method was used to synthesize bimetallic Ag-Au c nanoparticles, which were used to prepare a Ag-Au/PGV bentonite composite. Bimetallic Ag-AuNPs and their nanoclay composite were optically characterized using the scanning electron microscope, ultraviolet visible spectroscopy, X-ray diffraction, and Fourier transform infrared, whilst cyclic voltammetry (CV) and differential pulse voltammetry (DPV) were used to ascertain their electrochemical activity and properties. The results of surface morphological inspection showed an average size of 10 nm, in agreement with XRD. The bimetallic Ag-AuNPs UV/Vis characteristic wavelengths of 414 nm and 516 nm confirmed the presence of Ag and Au metals, respectively. XRD exhibited diffraction planes related to 2θ values of Ag and Au metals, whilst FTIR indicated mainly COO- functional groups from the citrate capping of bimetallic Ag-Au NPs. CV and DPV showed that bentonite nanoclay is largely insulated by silicates but exhibited a small electroactivity of Fe. The electroactivity of Ag-Au/PGV bentonite exhibited peak potentials due to Ag/Ag+ and Au/Au^{3+} redox couples at 0.19 V/−0.20 V and 1.37 V/0.42, respectively. The Ag-Au/PGV bentonite nanocomposite exhibited the highest surface concentration of 3.25×10^{-2} cm^2, a diffusion coefficient of 2.36×-11 cm^2/s, and an electron transfer rate constant (Ks) of 1.99×10^{-4} cm^2. The outcome of these results indicated that the Ag-Au/PGV bentonite nanocomposite was more electroactive than PGV. Therefore, this study accentuates Ag-Au/PGV bentonite nanocomposite as a novel and promising platform for electrochemical sensing with higher sensitivity and efficiency than other sensing materials.

1. Introduction

Bentonites are clays generally defined as montmorillonite (MMT), which is the basic and most abundant constituent of bentonite clay [1, 2]. Amongst other components, it consists of smectites, which are layers within the clay holding a negative charge. The layers contain species that include silicates and tetrahedrons that often contain metals such as magnesium, sodium, and iron. Bentonite presents strong colloidal properties, and its volume increases several times when encountering water, creating a gelatinous and viscous fluid [3]. The interesting properties of bentonite (hydration, swelling, water absorption, viscosity, and thixotropy) make it a valuable material for various uses and applications [3]. According to the literature, the large surface area of bentonite clay has led to its having enhanced catalytic properties, cation exchangeability, and chemical stability. Consequently, bentonite has been successfully used as a sensing material and in the fabrication of electrochemical sensors to determine pharmaceuticals and toxic metal ions [4]. Moreover, recent advancements have reported studies on bentonite modification for adsorption applications. Various materials have been used as modifiers from organic to inorganic substrates, and a recent study has reported bentonite coated with iron oxide forming a bentonite composite, which was used to remove pollutants in aqueous media [5]. However, the limitations associated with bentonite-ba bentonite-based electrochemical sensors have relatively low sensitivity due to on-transfer capacity.

Consequently, metal NPs have been used to functionalize such materials due to their good conductivity, plasmonic resonance, and high surface area, which overcome the limitations of surfaces that particularly exhibit poor electron transfer capacity. Nanoparticles with at least one dimension size of 10–100 nm may have various morphologies (amorphous, crystalline, spherical, needles, etc.) [6] and could be used in many applications because of their ability to self-assemble on the support surface. Two of the most common and most used monometallic nanoparticles (NPs) are silver (Ag) and gold (Au), with broad absorption bands in the visible zone that have been applied to modify electrode surfaces. AuNPs have previously been renowned for playing a substantial part in human welfare in clinical diagnostics, among other medical applications. However, recent research advancements have demonstrated the traction of AuNPs as they have become the most promising tool in the methods for cancer and antibacterial and AIDS treatments [7]. This is because the particle shape and size and nontoxic nature of AuNPs increase the permeability and retention effects that further suggest support for the informal accumulation and penetration in the treatment of tumor sites.

According to a recent study, significant active therapeutics for HIV treatment defined the status of AgNPs as a known HIV antiagent in the initial phase of viral duplication and later stages of the HIV life cycle [8]. Additionally, Ag and Au's metals have demonstrated excellent biocompatibility, optical properties, high surface area to volume ratio, and excellent conductivity [9]. Thus, AgNPs and AuNPs have been reported to be used as sensing materials in electrochemical studies of various pharmaceuticals, including ARVs.

The mixture of precious different metal elements within a small crystallite nanometer is also gaining increased attention due to their unique properties and can result in marked consequences [10]. Bimetallic precious nanoparticles have been shown to increase catalytic turnover rates in the practice of heterogeneous catalysis, improve selectivity, or enhance stability. From a scientific and technological point of view, bimetallic nanoparticles are of greater interest than corresponding monometallic ones due to their more intriguing properties. Nanocomposites based on clay minerals provide materials that have become key resources in pharmaceutical applications and have attracted considerable attention because of their great flexibility and improved properties [11].

Ag-Au bimetallic NPs compared to individual AgNPs and AuNPs are attracting greater attention in the biomedical field because of their antibacterial activity and in electrochemical analysis due to enhanced catalytic activity, surface area, and electron transfer [12]. Many electrochemical sensor platforms that possess fast, real time, and simple analysis have been proposed over conventional techniques for simple detection systems. Here, we fabricated a bentonite clay nanocomposite electrochemical sensor based on bimetallic Ag-AuNPs. As far as we know, no studies in the literature have ever mentioned this kind of sensor. The sensor showed enhanced conductivity, thermal stability, catalytic activity, and electrochemical properties. The characterization of the sensor was carried out by using cyclic voltammetry (CV) and differential pulse voltammetry (DPV) techniques to evaluate the effect of the nanocomposite on enhancing the peak current. Morphological structures were illustrated using a scanning electron microscope (SEM), and the molecular interaction occurring after the inclusion of bimetallic nanoparticles on clay was identified using Fourier transmittance infrared spectroscopy (FTIR). UV-VIS was also used for bimetallic Ag-AuNPs, and X-ray diffraction (XRD) was used for crystal structure, crystallite size, and strain X-ray diffraction patterns of the nanocomposite.

2. Experimental

2.1. Reagents and Materials. $AgNO_3$ (silver nitrate) (Aldrich, 99, 9%), $Na_3C_6H_5O_7$ (trisodium citrate) (Aldrich, 99%), $HAuCl_4$/chloroauric hydrate (99%, Aldrich), PGV-bentonite (99% Aldrich bentonite nanoclay), deionized water purified by the Milli-QMT system (Millipore), and hydrochloric acid (HCl, 99% Aldrich) were the following reagents and materials used in the experiment.

2.2. Synthesis of Ag-Au NPs. A coreduction chemical method was used to synthesize bimetallic NPs. 1 mM of both $AgNO_3$ and $HAuCl_4$ was mixed and made up in a 50 ml flask. The mixture was mildly boiled at 90°C, and then, trisodium citrate was added dropwise until a dark maroon/brown color occurred. This solution was placed to further heat for another hour and allowed to cool [7, 13].

2.3. Bentonite Clay Nanocomposite Preparation. The Ag-Au PGV-bentonite-functionalized nanocomposite was prepared by dispersing 1 g of PGV-bentonite in 100 ml of 1 mM $AgNO_3$ and $HAuCl_4$ solutions for 24 h. PGV-bentonite dispersions were centrifuged and dried at 105°C and, the exchanged Ag-Au PGV-bentonite nanocomposite was reduced by dispersing it in 2 mM of sodium citrate at boiling temperature. This process causes the dispersion of color to change from white to a brownish color [14].

2.4. Bare GCE Modification with Nanofilms. The glassy carbon electrode (GCE) was coated at separate times with Ag-Au bimetallic NPs and the Ag-Au/PGV bentonite composite, and throughout, the method that was used to coat was the drop-coating method [14]. Approximately 0.5 ml was cast on the bare GCE. The modified GCE was left to dry in an open vacuum for 2 hours.

2.5. Characterization Techniques

2.5.1. Scanning Electron Microscope (SEM). Scanning electron microscopy (SEM) images were acquired using Philips-FEI XL30 ESEM-TMP. The powdered samples were first affixed onto adhesive tapes supported on metallic disks and then covered with a thin, electrically conductive gold film. Images of metals and bentonite nanocomposite were

recorded at different magnifications at an operating voltage of 5.0 kV.

2.5.2. Ultraviolet-Visible Spectroscopy (UV/Vis). 1 ml approximately of Ag, Au monometallic NPs (1 mM), and Ag-Au (1 mM) bimetallic NPs was analyzed for characteristic absorbance peaks. The instrument that was used is the UV-1800-Shimadzu UV spectrophotometer, Advanced African Technology (Scientific division) serial number: 127471. Two quartz cuvettes were used, and one was used as a blank, hence containing only the solvent (Millipore water) and was used for baseline and background check. This was performed to eradicate noise and interference at the wavelengths of interest. The cuvettes were both inserted into the sample compartment, with one containing the solvent and another analyte (NPs), respectively. The scan was run, and spectra for each material were obtained and saved.

2.5.3. Fourier Transform Infrared Spectroscopy (FTIR). 0.5 ml of all NPs and nanocomposites was analyzed for characteristic vibrational and stretching bond peaks. The instrument that was used is PerkinElmer FTIR spectrum Two L1600300 spectrum two LITA, Serial number: 102561. The sample compartment was cleaned with low concentration alcohol (isopropanol) and a background scan was performed to clear noise and interference. Thereafter, 1 ml of each material was placed in the analyzing compartment, and the scan was taken sequentially. After a few seconds, the spectrum was obtained.

2.5.4. X-Ray Diffraction (XRD). The X-ray diffraction (XRD) studies of the NPs, PGV bentonite, and bentonite clay composites were performed by using a Bruker AXS D8 Advance diffractometer with Cu-Kα radiation over the scanning range $2\theta = 20^{\circ}$–90° at a voltage of 40 kV and 40 mA. All NPs and clay composites were in typically solid form. Approximately 2 mL of the nanoparticles was dropped on a copper plate.

2.5.5. Electrochemical Characterization. Cyclic and differential pulse voltammetric experiments were performed using AutoLab PGStat128 (MetrohmAutoLab) equipped with NOVA 2.1 Software (Metrohm AutoLab). The experimental setting was composed of conventional three electrode cells in which a saturated potassium chloride (KCl) electrode and a platinum wire were used as the reference (RE) and counter (CE) electrodes, respectively. Bare glassy carbon (GC) modified with Ag-Au NPs and Ag-Au/PGV bentonite films was used as a working electrode (WE). Before the modification, GC was sequentially polished with diamond powder (0.05, 0.3, and 1 μm, Sigma Aldrich) cloth and washed with Milli-*Q* water. Cyclic voltammetry was recorded in an aqueous solution with 0.1 M HCl as a supporting electrolyte. The CV data presented below were obtained at varying potential ranges against (Ag/AgCl), which depends upon the electro-oxidation electroreduction of each respective material nanoparticle, but the same scan rate, 70 mV/s. Due to the electrochemical plausible reversibility of redox couples observed at this scan rate, whilst voltammograms representing kinetics were obtained at a scan rate range of 10–90 mV/s.

3. Results and Discussion

3.1. Microscopic and Structural Characterization of the Nanomaterial

3.1.1. Scanning Electron Microscopy (SEM). The images shown in Figure 1 depict SEM images of pure PGV bentonite (a), Ag-AuNPs (b), and Ag-AuNPs/PGV (c) nanocomposite in 500 nm magnification with the insets in 5 μm magnification. The depiction outlines the morphological differences and their particle size distribution before and after Ag-AuNP functionalization of PGV bentonite.

Figure 1(a) depicts a large clumped-like structure of particles of PGV bentonite bound together with the majority in an average size of 20.97 nm, while Ag-AuNPs and Ag-AuNPs/PGV have the majority with an average diameter of 18.14, and 9.56 nm, respectively. The average sizes were measured using the Image *J* software and in agreement with the sizes confirmed by XRD, as seen in Table 1. The size of Ag-Au/PGV was smaller than that of PGV and Ag-AuNPs. An interesting phenomenon was also observed, whereby there was no sign of nanoparticles in the region of 60–80 nm for PGV, 100–140 nm for Ag-AuNPs, and 15–20 nm for Ag-AuNPs/PGV as shown in the corresponding histograms of the SEM images (a'–c'). Figure 1(c) shows the resemblance of both PGV bentonite and Ag-AuNPs, which confirmed the successful functionalization of PGV bentonite with Ag-AuNPs. A similar shape of particle size that was observed has been reported in surfactant property studies [15, 16]. The surface depicted by image (c) thus showed enhanced surface orientation of particles, which led to more electroactive sites within surface particle clusters compared to both PGV bentonite and Ag-AuNP [17].

3.1.2. UV/Vis Spectroscopy, X-Ray Diffraction, and Fourier Transform Infrared Spectroscopy (FTIR). Figure 2 shows the UV/Vis spectrum, FTIR, and XRD of the nanocomposite. The UV/Vis spectrum of Ag-AuNPs has shown that the maximum absorbing wavelengths at 414 nm and 516 nm are characteristics of Ag and Au metals, respectively, confirming the synthesis of Ag-Au NPs. These were the metal NPs that were used in the functionalization of bentonite clay, thus forming a bentonite clay composite.

According to the literature, Ag-AuNPs exhibit a plasmonic effect caused by the coalescent formation of NPs, thus exhibiting a characteristic wavelength range of 410–520 nm for Ag-AuNPs, and this range has been reported particularly for Ag-AuNPs existing in core-shell [18, 19]. The reported characteristic wavelengths by this study for the Ag-AuNPs were found to be 414 and 516 nm, within the reported wavelength range. Also, the data is in agreement with the studies done by Fernandez-LopeZ and co workers [14]. In support of the UV/Vis spectroscopic data, FTIR and XRD were conducted to verify the synthesis and functionalization

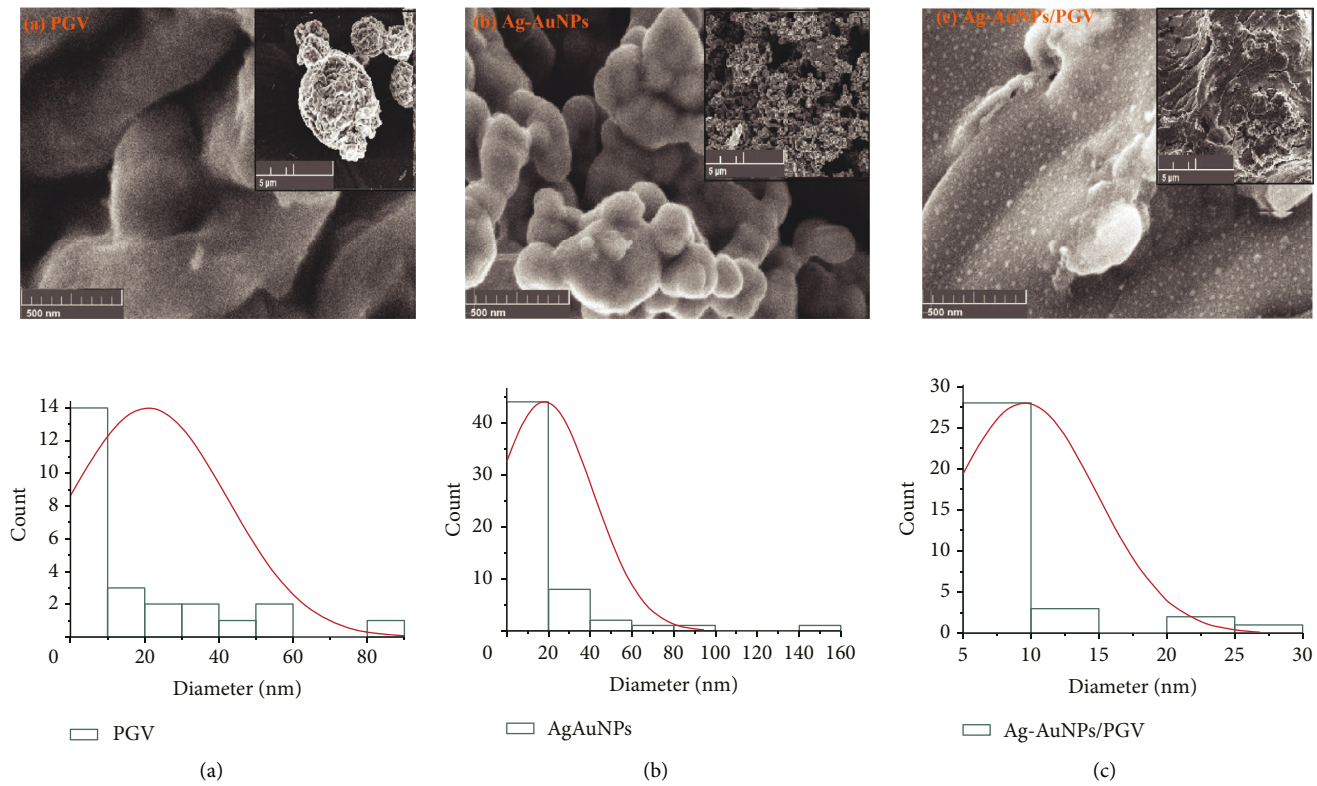

Figure 1: SEM images of PGV bentonite (a), Ag-AuNPs (b), and Ag-AuNPs/PGV bentonite (c) and corresponding distribution size histograms, PGV bentonite (a), Ag-AuNPs (b), and Ag-AuNPs/PGV bentonite (c). Inset: magnification of the SEM images at 5 μm.

Table 1: Comparison between the sizes of PGV, Ag-AuNPs, and Ag-AuNPs/PGV measured by SEM and XRD.

Sample	SEM (nm)	XRD (nm)
PGV	20.97	21.51
Ag-AuNPs	18.14	19.75
Ag-AuNPs/PGV	9.56	10.42

of bentonite clay composites from bimetallic Ag-AuNPs. The results of the characterization in functionalization are depicted in Figures 2(b) and 1(c). The FTIR spectral peaks depicted in Figure 2(b) are an indication of the spectra of PGV, Ag-AuNPs/PGV, and citrate-capped Ag-AuNPs.

Comparable FTIR spectra of PGV bentonite, Ag-AuNPs, and Ag-AuNPs/PGV showed the presence of the bunch of the OH group and N-H extending of amine gathering that can be manifested in the region of 3237, 3328, and 3327 cm, respectively, related to the presence of adsorbed water [20]. Moreover, the absorption bands depicted by both C=O and COO- functional groups inbothAuNPs and Au NPshave been reported in the literture to be optically active around 1580–1650 cm^{-1} and 1050–1380 cm^{-1}, respectively [16, 21]. There was a further depiction of spectral peaks mainly from bentonite clay, and other peaks indicated that they were due to mostly silicates. The peaks observed for bentonite clay in this study were similar to those observed in the study by Reddy and et al. [3]. The peaks indicated by *m*, *k*, and *q* are due to components of bentonite clay and are exhibited by nanocomposites and have been reported to be in a similar diffraction plane [1, 17].

In correlation with the spectra of PGV or Ag-AuNP samples to Ag-AuNPs/PGV, some bands decrease and others shift, such as the peak of Si-O-Si stretching frequencies at 1067 cm^{-1} of Si-O-Si. This is the result of the binding of bimetallic with clay and affects the Si-O vibrations. This confirmed that bentonite clay used in this study has similar optical properties as those reported in the literature. The Ag-Au bentonite clay composite exhibited some of the main peaks that are observed in Figure 1(b), particularly the COO- and C=O functional groups caused by the citrate capping agent and carbonyl groups, which perform a reduction of metal ions within clay composites according to the study of biogenic reducing agents. Thus, the data confirmed that PGV bentonite had been successfully functionalized with bimetallic Ag-AuNPs.

A comparative analysis of the XRD patterns of the synthesized material is shown in Figure 1(c), and the crystallographic parameters were evaluated. Given the XRD spectra of the PGV sample in Figure 2(c), montmorillonite is confirmed as the most prevailing component. Phase analysis of the PGV showed some peaks of impurities of quartz and kaolinite in addition to montmorillonite. The peaks at 467 cm^{-1}, 517 cm^{-1}, 783 cm^{-1}, and 1120 cm^{-1} point to the presence of quartz (Si-O-Si), while the bands at 1034 cm^{-1} and 1634 cm^{-1} reveal the presence of amorphous SiO_2. These results justify an earlier report of quartz, which was confirmed by FTIR, and are in similar agreement with the XRD

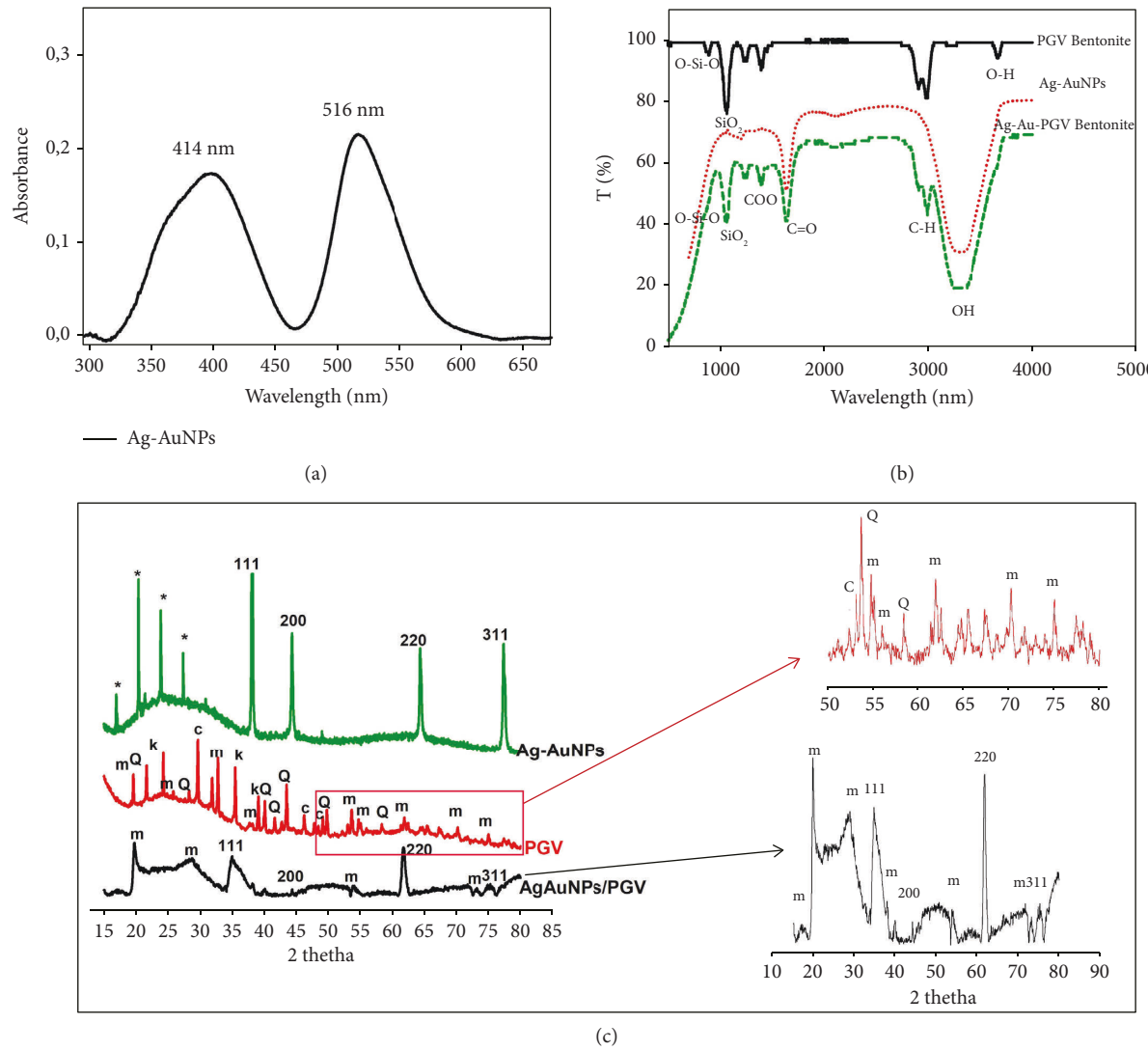

Figure 2: Presentation of UV/Vis of Ag-AuNPs (a), overlayed FTIR of PGV bentonite, Ag-AuNPs, Ag-AuNP-PGV (b), and overlayed XRD of PGV bentonite, Ag-AuNPs, and Ag-AuNPs/PGV bentonite with inset showing tiny peaks of PGV and Ag-AuNPs/PGV (c).

studies performed by Silva et al. [22]. The diffraction peaks indicated by Ag-AuNPs have diffraction planes of (111), (200), (220), and (311), which are related to 2θ values of 38.30, 44.40, 64.50, and 77.50. The high intensity of the 111-diffraction plane is an indication of the orientation of Ag and Au in nanoparticles. The impurities of the Ag-AuNP sample were marked with asterisks. These diffraction planes and corresponding 2θ values indicate AgNPs but do resemble AuNPs as well due to the similar plasmonic nature of the two metals [23]. Similar diffraction planes correspond to the same 2θ values as those observed for Ag-AuNPs, although there is a slight shift and are different intensities due to the matrix effect caused by bentonite clay on metals. The crystalline sizes of these samples were calculated using Debye-Scherer's equation $D = 0.9\lambda/\beta \cos\theta$, where D is the crystalline size, λ is the wavelength of X-ray, β is the full width at half maximum of the diffraction peak, and θ is Bragg's angle. The average sizes obtained for PGV, Ag-AuNPs, and Ag-AuNPs/PGV are estimated to be around 21.51, 19.75, and 10.42 nm, respectively. Table 1 shows the average sizes obtained by XRD in agreement with sizes obtained by SEM. The XRD pattern diffractions depicted in Figure 1(c) indicate that PGV bentonite has been functionalized with Ag-AuNPs.

3.2. Electrochemical Studies

3.2.1. Cyclic Voltammetry and Differential Pulse Voltammetry Behaviour of Ag-Au Bentonite Clay Composite. The voltammograms depicted in Figure 2 are CVs and DPVs of PGV, Ag-Au NPs, and Ag-Au-functionalized bentonite clay composite coated on the GCE. These voltammograms depict the electrochemical behaviour of Ag-AuNPs and Ag-Au/PGV bentonite-functionalized composites at the potential ranges of −0.5 V to 1.5 V, 0.75 to 2 V, and −0.5 V to 2 V Ag/AgCl, respectively. The electroactivity of the Ag-Au/PGV bentonite nanocomposite exhibited a pair of peak potential redox couples at 0.19 V/−0.20 V and 1.37 V/0.42 V vs. Ag/AgCl that are due to Ag/Ag^{+} and Au/Au^{3+}, respectively. The oxidation peak at 0.19 V and the reduction peak at −0.20 V vs. Ag/AgCl have been reported previously with

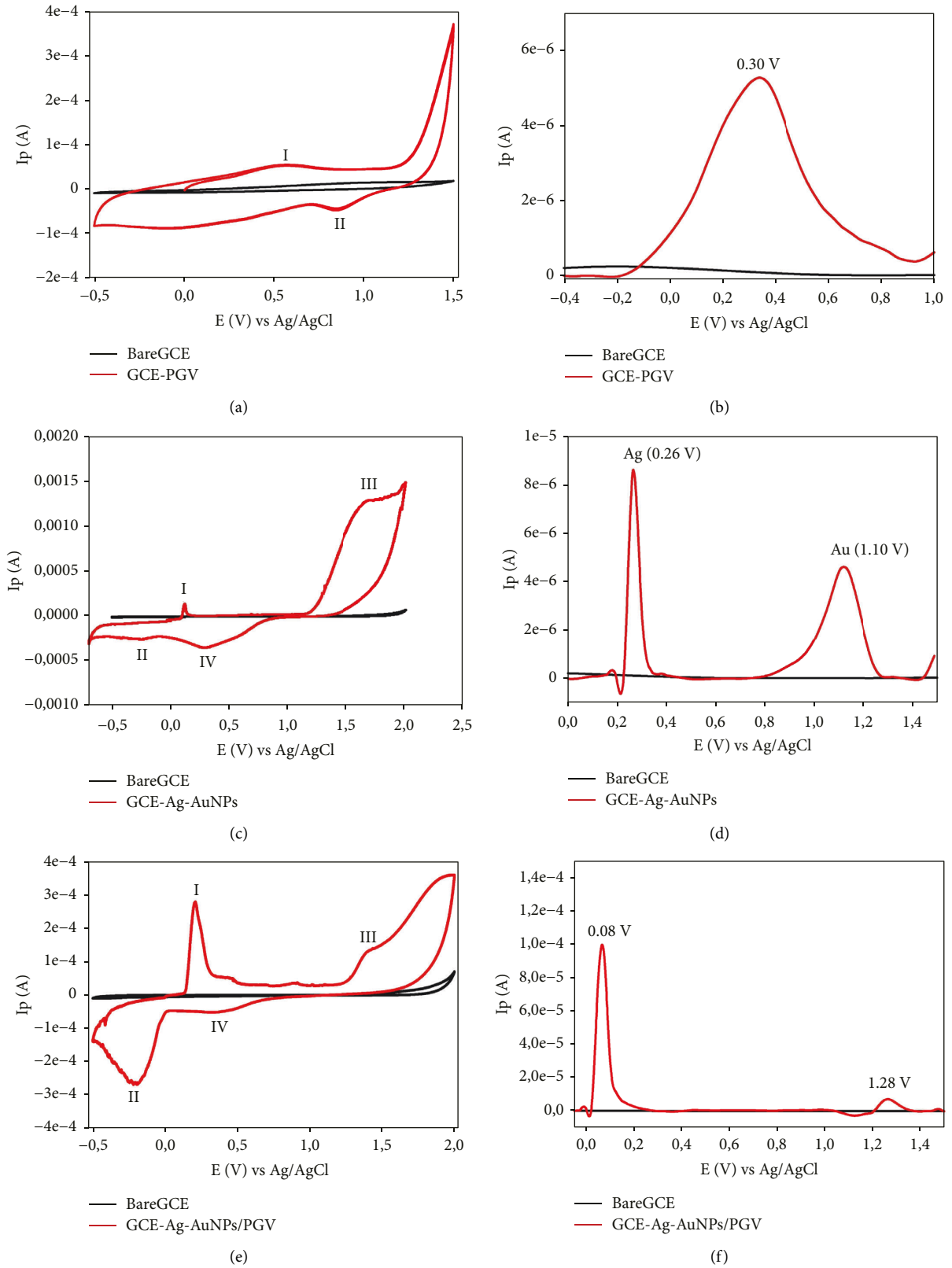

Figure 3: CV and DPV voltammetric data of PGV bentonite (a, b), Ag-AuNPs (c, d), and Ag-AuNPs/PGV (e, f) bentonite depicting the difference in electrochemical behavior caused by bentonite functionalization obtained in the 0.1 M HCl supporting electrolyte at a CV scan rate of 70 mv/s, and 0.035 V and 15 s DPV pulse amplitude and condition time, respectively.

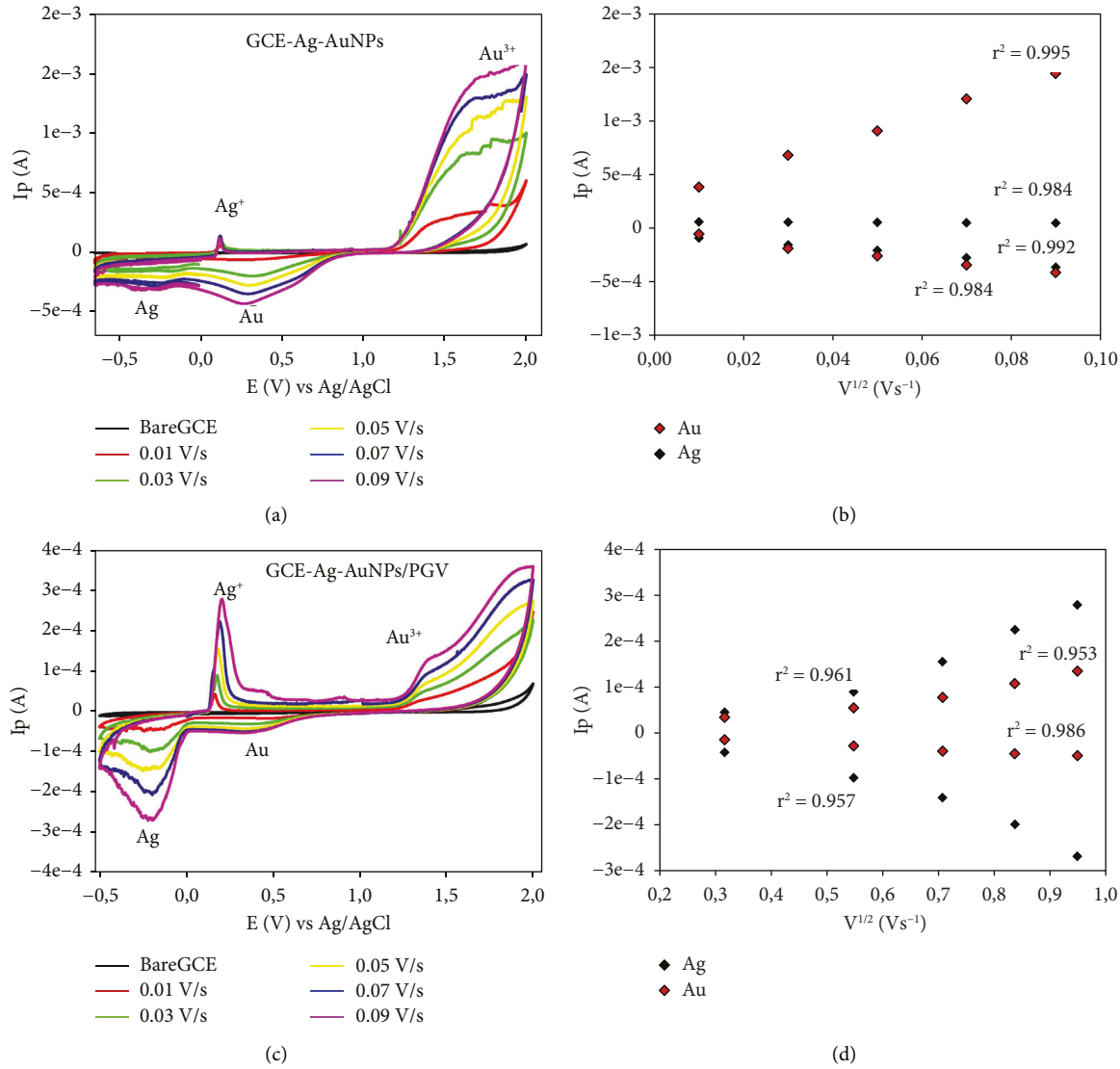

Figure 4: Overlay of various scan rates studies (a, c) for bimetallic and bimetallic bentonite composite, respectively. Randle's linear dependence plots (b, d) for Ag-AuNPs and Ag-Au/PGV bentonite, respectively, in the 0.1 M HCl supporting electrolyte.

similar behaviour [8, 9, 24], and the redox couple of Au at potentials 1.37 V/0.42 V vs. Ag/AgCl is in close agreement with literature studies [3, 21]. No response was observed in both CV and DPV of GCE in 0.01 M HCl electrolyte solution. The electroactivity of Ag-AuNPs is indicated by I and II (Ag^+/Ag) and III and IV (Au^{3+}/Au), respectively, as electroactive species for both Ag-Au NPs and the respective bentonite composite. Figure 3(a) depicts minute electroactivity of PGV bentonite clay due to the iron redox couple at potentials 0.3 V/0.8 V vs. Ag/AgCl and corresponding DPV-confirmed iron electroactivity.

The oxidation/reduction peak potentials that were observed in this study for Ag and Au species within the bimetallic system were in accordance with those observed for Ag-Au alloys, which were reported in a study of aptasensing of bacterial cells [5, 24]. Based on the CV and DPV voltammograms depicted in Figures 3(a) and 3(d), the Au metal appeared less reactive than Ag due to its lower oxidation peak intensity and potential, which agreed with the findings reported in the p-nitro reduction using Ag-Au alloy NP study [4, 17].

Furthermore, as evidenced by the successful Ag-AuNP functionalization of bentonite clay, DPV and CV voltammograms observed in Figures2(e) and 2(f) depicted potential peaks that are characteristics of Ag and Au metals. The slight negative potential shifts observed for Ag^+/Ag and Au^{3+}/Au species can be ascribed to the functionalization of bentonite clay, which enhanced the electrochemical activity of both metals, as peak intensities of these metals were enhanced significantly compared to those observed in Figures 2(b) and 2(c).

3.2.2. Kinetic Studies. The investigative study on the effect of scan rates on the electroactivity and electron transfer processes of bimetallic (AG-AuNPs) and the Ag-Au/PGV bentonite composite with their corresponding Randles–Sevcik linear dependency plot figures are shown in Figures 4(a)–4(d). The scan rate studies serve as diagnostic criteria for differentiating the steps of the reactions that occur at the surface of the electrode.

Table 2: Presentation of obtained Randles–Sevcik properties of Ag-AuNPs and Ag-Au/PGV bentonite composite.

Sample	n-electrons	De ($cm^2 \cdot s^1$)	Γ ($mol \cdot cm^{-1}$) $\times 10^{-2}$	K_S (s^{-1}) $\times 10^{-4}$
Ag-AuNPs	1.66	5.06×10^{-12}	1.15	2.87
Ag-Au-PGV	0.70	2.36×10^{-11}	3.25	1.99

The peak current densities of Ag-Au/PGV bentonite increased by greater margins compared to those of Ag-Au NPs, which indicated the electrochemical effect caused by the functionalization of PGV bentonite caused by Ag-AuNPs as the electroactivity of bentonite was significantly enhanced. The changes in the peak potentials of both Ag-AuNPs and Ag-Au/PGV bentonite depicted by voltammograms shifted minutely as the scan rate increased.

According to the Randles–Sevcik equation, a linear relationship occurs between the peak current (Ip) of freely diffusing reversible electrochemical redox species and the square root of its scan rate. Following the Randles–Sevcik suggestion, the effect of scan rates on both Ag-Au NPs (Figure 4(b)) and Ag-Au/PGV (Figure 4(c)) bentonite deviated, exhibiting values lower than those expected, which is the characteristic of quasi-reversible and adsorption control systems. This observation was also supported by the plot of In Ip vs. Inv (not shown), which gave a slope close to 1 for both Ag-Au bimetallic nanoparticles and their nanocomposite.

Table 2 shows that Ag-Au-PGV undergoes a one-electron reaction at the GCE in 0.1 M HCl, while Ag-AuNPs undergo a two-electron reaction. The surface coverage of $3.25 \times 10^{-2}\,cm^2$ depicted by Ag-Au/PGV bentonite is greater than $1.15 \times 10^{-2}\,cm^2$ depicted by bimetallic Ag-AuNPs. This confirmed that the functionalization of bentonite clay with Ag-AuNP films caused the surface volume of bentonite clay to increase significantly, thus forming a bentonite composite with more electroactive sites compared to bimetallic Ag-AuNPs films. Additionally, the electron transfer rate constant of bimetallic Ag-Au/PGV bentonite was significantly lower than that of bimetallic Ag-AuNPs. The value of the diffusion coefficient (De) was found to be in the order Ag-AuNPs/PGV > Ag-AuNPs. This indicates that electron diffusion was the slowest in bimetallic nanoparticles. This was an indication of the bentonite clay functionalization electrochemical effect on bimetallic Ag-AuNPs, and the electrochemical efficiency of Ag-Au/PGV bentonite was greater than that of bimetallic Ag-AuNPs. In agreement with many previous publications, similar electrochemical enhancements of supported Ag-Au bimetallic nanoparticles have been reported [16, 25]. The effects were observed as the surface area of the electroactive species significantly increased due to supporting material. Additionally, bimetallic and nanocomposites have been recently used in environmental and biomedical applications with better surface areas and diffusion coefficients [26]. Moreover, the correlation factors (R^2) for both Ag-AuNPs and Ag-Au/PGV bentonite indicated that the data were statistically reliable and acceptable.

4. Conclusion

This study is designed to synthesize a Ag-Au/PGV bentonite nanocomposite as a promising new structural material that can be used for sensing purposes. The desirable structural and electrochemical properties of PGV bentonite, AgNPs, Ag-AuNPs, and Ag-Au/PGV bentonite nanocomposite were successfully achieved by combining complementary techniques such as SEM, FTIR, UV-VIS, XRD, CV, and DPV. The particle sizes of the nanocomposite were smaller than those of pure clay and bimetallic nanoparticles, with an average size of ~10 nm, as observed on SEM. The UV-Vis studies of bimetallic Ag-AuNPs exhibit strong LSPR bands of 416 and 519 nm, which is an indication of nanoparticle formation. The FTIR spectrum and XRD results of the Ag-Au/PGV bentonite nanocomposite provide strong evidence of the incorporation of clay into the bimetallic nanoparticles. The electrochemical properties of the glassy carbon electrode modified with nanocomposites reveal the efficiency of Ag-Au/PGV bentonite with a more significant current response than that of PGV and bimetallic Ag-AuNPs. The findings of this study confirmed that the functionalization of bentonite clay with Ag-Au NPs improved the surface and electrochemical properties of bentonite clay. These reported data indicate that the functionalization of bentonite with metallic NPs can be used as an alternative method to improve the surface electrochemical capacity of bentonite and its application as an efficient sensing material for electrochemical sensors.

Data Availability

The data can be obtained from the corresponding author upon request.

Conflicts of Interest

The authors declare that they have no conflicts of interest.

Acknowledgments

The authors are extremely thankful for the funding provided by CPUT and NRF (grant (116237)) for carrying out the study.

References

[1] S. L. Abdullahi and A. A. Audu, "Comparative analysis of the chemical composition of bentonite clays obtained from Ashaka and tango deposits in Gombe state, Nigeria," *Chemical Search Journal*, vol. 8, no. 2, pp. 35–40, 2017.

[2] C. Aguzzi, P. Cerezo, C. Viseras, and C. Caramella, "Use of clays as drug delivery systems: possibilities and limitations," *Applied Clay Science*, vol. 36, no. 1-3, pp. 22–36, 2007.

[3] T. R. Reddy, S. Kaneko, T. Endo, and S. L. Reddy, "Spectroscopic characterization of bentonite," *Journal of Lasers, Optics & Photonics*, vol. 4, p. 171, 2017.

[4] P. K. Rastogi, D. K. Yadav, S. Pandey, V. Ganesan, P. K. Sonkar, and R. Gupta, "Synthesis and characterization of gold nanoparticles incorporated bentonite clay for

electrocatalytic sensing of arsenic (III)," *Journal of Chemical Sciences*, vol. 128, no. 3, pp. 349–356, 2016.

[5] P. R. Vernekar, N. P. Shetti, M. M. Shanbhag, S. J. Malode, R. S. Malladi, and K. R. Reddy, "Novel layered structured bentonite clay-based electrodes for electrochemical sensor applications," *Microchemical Journal*, vol. 159, Article ID 105441, 2020.

[6] A. Murugan, K. Kumara, and Shanmugasundaram, "Biosynthesis and characterization of silver nanoparticles using the aqueous extract of vitex negundo," *World Journal of Pharmacy and Pharmaceutical Sciences*, vol. 3, no. 8, 2014.

[7] C. Garrido, C. Simpson, and J. Bresse, "Gold nanoparticles to improve HIV drug delivery," *Future Medicinal Chemistry*, vol. 7, no. 9, 2015.

[8] A. Bowen, E. E. Sweeney, and R. Fernandes, "Nanoparticle-based immunoengineered approaches for combating HIV," *Frontiers in Immunology*, vol. 9, 2020.

[9] S. N. Mailu, T. T. Waryo, P. M. Ndangili et al., "Determination of anthracene on Ag-Au alloy nanoparticles/overoxidized-polypyrrole composite modified glassy carbon electrodes," *Sensors*, vol. 10, no. 10, pp. 9449–9465, 2010.

[10] S. V. Belenov, V. A. Volochaev, V. V. Pryadchenko et al., "Phase behavior of Pt-Cu nanoparticles with different architecture upon their thermal treatment," *Nanotechnologies in Russia*, vol. 12, no. 3-4, pp. 147–155, 2017.

[11] C. Yu, K. Yang, Y. Xie et al., "Novel hollow Pt-ZnO nanocomposite microspheres with hierarchical structure and enhanced photocatalytic activity and stability," *Nanoscale*, vol. 5, no. 5, p. 2142, 2013.

[12] Y. J. Choi and T. J. M. Luo, "Electrochemical properties of silver nanoparticle doped aminosilica nanocomposite," *International Journal of Electrochemistry*, vol. 2011, pp. 1–6, Article ID 404937, 2011.

[13] E. Hamidi-Asl, F. Dardenne, S. Pilehvar, R. Blust, and K. De Wael, "Unique properties of core shell Ag@ Au nanoparticles for the aptasensing of bacterial cells," *Chemosensors*, vol. 4, no. 3, 2016.

[14] K. Shameli, M. Bin Ahmad, M. Zargar et al., "Synthesis and characterization of silver/montmorillonite/chitosan bionanocomposites by chemical reduction method and their antibacterial activity," *International Journal of Nanomedicine*, vol. 6, pp. 271–284, 2011.

[15] C. Anastasios, M. Antonio, F. Causa, G. Romeoa, and A. P. Nett, "Bimetallic Au/Ag nanoparticle loading on PNIPAAm-VAA-CS8 thermoresponsive hydrogel surfaces using ss-DNA coupling, and their SERS efficiency," *Royal Society Chemistry Advance*, vol. 5, 2015.

[16] N. S. Awwad, M. A. El-Kader, H. A. Ibrahium, G. M. Asnag, and M. A. Morsi, "Green synthesis of different ratios from bimetallic gold: silver nanoparticles core@shell via laser ablation scattered in Chitosan-PVA matrix and its electrical conductivity behavior," *Composites Communications*, vol. 24, Article ID 100678, 2021.

[17] M. Khan, K. Al-Hamoud, Z. Liaqat et al., "Synthesis of Au, Ag, and Au-Ag bimetallic nanoparticles using pulicaria undulata extract and their catalytic activity for the reduction of 4-nitrophenol," *Nanomaterials*, vol. 10, no. 9, 2020.

[18] D. K. Lim, I. J. Kim, and J. M. Nam, "DNA-embedded Au/Ag core-shell nanoparticles," *Chemical Communications*, vol. 42, 2008.

[19] E. N. Saw, V. Grasmik, C. Rurainsky, M. Epple, and K. Tschulik, "Electrochemistry at single bimetallic nanoparticles-using nano impacts for sizing and compositional analysis of individual AgAu alloy nanoparticles," *Faraday Discussions*, vol. 193, pp. 327–338, 2016.

[20] D. Malina, A. Sobczak-Kupiec, Z. Wzorek, and Z. Kowalski, "Silver nanoparticles synthesis with different concentrations of polyvinylpyrrolidone," *Digest Journal of Nanomaterials and Biostructures*, vol. 7, 2012.

[21] Y. Matsui, K. Hamamoto, Y. Kitazumi, O. Shirai, K. Kano, and K. Kano, "Diffusion-controlled mediated electron transfer-type bioelectrocatalysis using microband electrodes as ultimate amperometric glucose sensors," *Analytical Sciences*, vol. 33, no. 7, pp. 845–851, 2017.

[22] I. A. Silva, J. M. R. Costa, R. R. Menezes, H. S. Ferreira, G. A. Neves, and H. C. Ferreira, "Studies of new occurrences of bentonite clays of the state of paraiba for use in water-based drilling fluids," *Mining, Revista Escola de Minas*, vol. 485, p. 66, 2013.

[23] A. Amargeetha and S. Velavan, "X-ray diffraction (XRD) and energy dispersive spectroscopy (EDS), analysis of silver nanoparticles synthesized from erythrina indica flowers," *Nanoscience and Technology*, vol. 5, pp. 1–5, 2018.

[24] G. P. Shevchenko, V. A. Zhuravkov, and G. V. Shishko, "A one-pot synthesis of colloidal Ag-Au nanoparticles with controlled composition," *SN Applied Sciences*, vol. 1, no. 10, pp. 1192–1196, 2019.

[25] M. Bücker, A. F. Orozco, and A. Kemna, "Electrochemical polarization around metallic particles—part 1: the role of diffuse-layer and volume-diffusion relaxation," *Geophysics*, vol. 83, no. 4, pp. E203–E217, 2018.

[26] C. Fernández-López, L. Polavarapu, D. M. Solís et al., "Gold nanorod-pnipam hybrids with reversible plasmon coupling: synthesis, modeling, and sers properties," *ACS Applied Materials and Interfaces*, vol. 7, no. 23, pp. 12530–12538, 2015.